P2-85

Video tracking and post-mortem analysis of dust particles from all tungsten ASDEX-Upgrade

N. Endstrasser[1], F. Brochard[2], V. Rohde[1,*], M. Balden[1], T. Lunt[1], S. Bardin[2], J-L. Briançon[2], R. Neu[1] and the ASDEX Upgrade Team[1]

[1]*Max-Planck-Insitut für Plasmaphysik,EURATOM Association, Boltzmannstrasse 2, D-85748 Garching, Germany.*

[2]*Institut Jean Lamour, Nancy-Université, Bvd. des Aiguillettes,F-54506 Vandoeuvre, France.*

Abstract

2D dust particle trajectories are extracted from fast framing camera videos of ASDEX-Upgrade (AUG) by a new time- and resource-efficient code and classified into stationary hot spots, single-frame events and real dust particle fly-bys. Using hybrid global and local intensity thresholding and linear trajectory extrapolation individual particles could be tracked up to 80 ms. Even under challenging conditions such as high particle density and strong vacuum vessel illumination all particles detected for more than 50 frames are tracked correctly. During campaign 2009 dust has been trapped on 5 silicon wafer dust collectors strategically positioned within the vacuum vessel of the full tungsten AUG. Characterisation of the outer morphology and determination of the elemental composition of 5×10^4 particles were performed via automated

PACS: 28.52.Nh, 82.80.Ej, 68.37.Hk
JNM keywords: Electron Microscopy, Plasma-Materials Interaction, Safety of Nuclear Reactors and Components, Tungsten, Tungsten Alloys and Compounds, Mathematical and Computational Methods
PSI-19 keywords: ASDEX-Upgrade, Dust, Particle control, Scanning electron microscopy, Tungsten
[*] *Corresponding author address:* Boltzmannstr. 2, 85748 Garching b. München, Germany.
[*] *Corresponding author E-mail:* Volker.Rohde@ipp.mpg.de
Presenting author: Nikolaus Endstrasser
Presenting author e-mail: Nikolaus.Endstrasser@ipp.mpg.de

SEM-EDX analysis. A dust classification scheme based on these parameters was defined with the goal to link the particles to their most probable production sites.

1. Introduction

In order to characterize the impact of dust on the plasma performance and operation and to quantify the dust generation rates during plasma operation in tokamaks, camera observations of dust particle transport and quantification of characteristic tokamak dust parameters [1-3] are crucial for the realization of reliable model predictions. The probability for the penetration of a specific dust grain, e.g. into the confined inner plasma depends on its trajectory and life-time [4,5] influenced by its elemental composition and outer morphology [6]. Furthermore, the dust composition observed in present-day tokamaks is required for laboratory studies on dust mobilization [7] and chemical reactivity [8] aiming at a reliable assessment of the risks emerging from loss of vacuum or coolant leakage accidents such as long range transport of tritium by mobilized dust or damage of in-vessel components during an explosion of accumulated dust.

The paper describes two methods now established at ASDEX-Upgrade (AUG) for obtaining quantitative data on dust generation and transport. One aims to determine particle trajectories from fast framing camera videos by an algorithm allowing statistical analysis of recorded dust events. The other method delivers a classification of collected dust regarding their chemical composition and morphology by automated analysis of a huge number of particles.

2. Experimental

2.1 Fast Camera

In order to investigate the link between discharge conditions and dust production and transport in AUG, dust particle migration in the tokamak was monitored using fast framing cameras. For the statistical analysis of the thereby gained 8 GB videos with 10000 fps, 256 × 256 px resolution and 14 bit depth resolution, an algorithm for fully automated movie analysis was developed. Analysis of AUG movies showed that at this frame rate the mean displacement of moving dust particles is 0.3 px per frame allowing extraction of accurate trajectories. In order to benchmark the efficiency of different implemented detection and tracking routines a dedicated experiment was performed in a laboratory device. Therein, the oscillation of

carbonaceous dust particles with the frequency of the periodical expansion of the particle confining cathode sheath of a parallel plate RF discharge was monitored with a camera (for details see [11,12]). As the main characteristics of individual trajectories are known a priori and movies with similar features as those observed in tokamak disruptions, i.e. a very large particle numbers, strong light intensity variations and experimental noise, were obtained, the particle detection efficiency of the algorithm could be assessed. The thereby qualified code was then used for automated analysis of AUG videos recorded during the previous AUG campaign.

2.2 Dust collection

In addition to the in-situ tracking of dust, five silicon wafer dust collectors were mounted in AUG in 2009 for post-mortem analysis of deposited dust. The dust was collected on 45×20 mm sized silicon wafer pieces mounted in protective stainless steel housings. Contamination of the silicon wafers with airborne dust particles and aerosols was minimized by sealing the casings immediately after vessel opening. Particle detection was performed by a commercial software using grey-scale thresholding of secondary electron images recorded with a FEG-SEM at an electron energy of 15 kV. To obtain reliable data only particles composed of at least 16 px corresponding to an equivalent circle diameter (ECD) of 0.28 µm were taken into account for analysis. No further morphological image processing was performed to avoid unpredictable biasing of the particle morphological parameters. Particle classification was performed using both, their outer morphology determined by evaluation of the greyscale SEM images and their elemental composition extracted from EDX spectra recorded for 15 s for each particle. Area number densities and coverage fractions for each class observed in AUG are presented in the following section.

3. Analysis Techniques

3.1 Particle detection and trajectory extraction

The newly developed algorithm described in detail in [11] and [12] is divided into the detection of individual dust grains in each frame and the connection of individual dust particle locations to complete trajectories. Due to thermal radiation, dust particles appear as bright spots in front of an inhomogeneous background. Thus, particles can be detected by identification of local intensity peaks. Two different techniques were compared. In the first one, band-pass filtering is first applied to each frame, in order to eliminate structures of PFCs with a high surface roughness illuminated during e.g. plasma bursts or reflections as well as pixel-size noise (caused by thermal noise on camera CMOS sensor). Local intensity peaks are found by applying automatic global thresholding without background image substraction as described by Yu et al. [13] and Boeglin et al. [14] allowing the detection of stationary events such as hot spots. With the second technique, intensity peaks have to satisfy both a global threshold, and a local one defined for each pixel as a function of its neighbours in order to be considered as potential particles. This second technique, called hybrid global/local thresholding in this contribution, does not require preliminary filtering, it lowers the number of misdetections but is also about 30 times more time consuming (see Fig. 1). More explanations on thresholding techniques can be found in the survey from Sezgin and Sankur [15]. In order to link successive positions of detected particles, in the consecutive frames all particles registered within the range of the displacement diameter (DM) of 5 px relative to the previous particle position are identified. The most probable subsequent particle position is thereby the one with the minimum total squared displacement from its previous position. Although even higher displacements of fast particles were observed than the maximum authorized DM of 5 px, which is quite large compared to the determined average particle displacement, higher DM values are not suitable as they may cause confusion between close particles as well as longer computation times. The algorithm subsequently generates a synthetic table containing a list of all identified events, and their successive coordinates in all frames where they are detected. Based on their tracking duration and maximal

displacement, events are then automatically classified as real dust particles fly-bys, hot spots, or single frame events such as neutrons interacting with the image guide or arc events.

3.2 Particle Identification Parameters

As three morphological parameters were used for the definition of dust classes with different outer morphology, their purpose will shortly be explained here. The equivalent circle diameter (ECD), i.e. the diameter of a circle with an area corresponding to the projected particle area, is commonly used to describe spheroid particles. The elongation of a particle can accurately be described calculating the ratio of the greatest to the least feret diameter. Particle shapes with a feret aspect ratio close to 1 have a circular appearance. Due to geometric considerations the smallest particles included in the analysis with an area size of 16 px and an aspect ratio up to 1.18 have to be considered circular. Therefore, in the present study all tungsten-dominated particles with an aspect ratio between 1 and 1.18 were considered as droplets and the rest attributed to the class of tungsten-dominated flakes. The shape can be described by the ratio of the area calculated from the particle perimeter and the measured projected area. A shape value of 1 corresponds to a perfect circle, while large values indicate particles with high surface roughness or large elongation. Equally sized features with a differently smooth borders can be separated due to their diverging shape value, e.g. as manual analysis of morphological data has shown smoothly shaped boron crystallites could be separated from flakes with a comparable elemental composition by their shape value higher than 1.2.

4. Results and discussion

4.1 Validation of tracking algorithm

Overlaying of the obtained trajectories onto the images of the raw movies is the most intuitive approach to assess the detection efficiency of the code, but does not provide a quantitative evaluation of its performance. Thus, a dedicated laboratory setup described in the experimental section was used for the production of benchmark videos with very large particle numbers, strong light intensity variations and experimental noise. A simple estimate of the code

efficiency under these artificially produced extreme conditions is then provided by computing the cross-correlation between individual particles trajectories and the sheath fluctuations. Results showed that particles with a correlation higher than 70 % were correctly tracked, while below 60 % many trajectories were erroneous, generally due to confusion between particles in close vicinity to each other. Evaluation of the registered particle trajectories according to this method revealed that all particles tracked for more than 50 frames (i.e. one period of oscillations) were correctly identified. Although direct comparison of benchmark movies and tokamak discharge videos is difficult due to the toroidal symmetry reducing in AUG movies the amount of particles being in view of the camera for more than 50 frames (see insert in Fig. 1), manual verification of the results indicates that the ratio of correctly tracked particles is higher for AUG movies recorded under comparable background intensity variation conditions. Therefore, the experimental benchmark procedure may deliver underestimated values for the particle detection and tracking efficiency.

Applying this analysis technique to the recorded video tracking data of AUG will allow in the future to obtain statistically relevant data about dust events, their temporal distribution in each discharge and during the experimental campaigns.

4.2 Particle classification

A detailed overview of the particle coverage in registered particles per mm^2 and in % of the sampled area covered by dust particles detected on the indicated area of silicon wafers no. 1, 3, 4 and 5 is given in Fig. 2. Data from wafer no. 2 installed close to the glow discharge anode were excluded from this study as on its surface micrometer thick, partially ablated deposits predominantly composed from boron and iron were formed obviously directly during the boronizations leading to a topography rich in contrast in SEM.

In the left graph of Fig. 2 the total particle area number density is given in mm^{-2} on top of the columns representing the fractional wafer dust compositions. In comparison to the other three positions the density of particles seems to be remarkably increased for wafer no. 1 situated at the

central column below the inner heat shield. This can be explained by the high yield of silicon dominated fibres there probably released from the glass fibre insulation wrapped around cables of plasma diagnostics moving during plasma operation. Therefore, the untypically high particle coverage on wafer no. 1 can be explained as a consequence of a high contribution of debris, i.e. particles not produced by direct plasma interaction processes. In order to gain correct particle statistics, the contribution of debris and particles of organic origin i.e. particles containing elements forming salts such as Na, K and Ca and S, were depicted as contaminants in Fig. 2. All particles of organic origin are considered contaminants as they originate from previous in-vessel maintenance works. Based on their elemental composition further differentiation of particles was carried out leading to the definition of the seven highest abundant particle classes contributing at least for one of the wafers 5 % of the total amount of registered particles on the sampled areas: tungsten-dominated flakes and droplets (including also spherically shaped particles with negligible contributions of titanium, iron, nickel and chromium), carbon-dominated flakes, boron crystallites and flakes, iron-dominated droplets and copper flakes. Boron particles were already previously observed on silicon wafers extracted after the 2007 and 2008 campaign [3]. Differentiation into flakes and crystallites seemed necessary as they obviously were formed by different processes: while boron crystallites grow uniformly on all previously boron coated areas after contact to water vapour, flakes are formed by the ablation of boron coatings e.g. due to thermal stress during the plasma operation.

The contribution of each of the eight classes in Fig. 2 is given as relative frequency (left graph) and fraction of the total particle covered area in % (right graph), showing that tungsten, carbon and boron containing dust particles are predominant in the boronized all-tungsten AUG in terms of area number density and coverage fraction. Wafer no. 1 shows besides the high contribution of debris and other contaminants already discussed above, comparatively high values for the area number density and coverage fraction of carbon flakes, while for the tungsten-dominated particles they are comparatively low. Considering the mounting position of this

collector below the heat shield, the largest fraction of carbon dust is produced by the constant movement of the heat shield tiles during plasma operation, while these tiles shield the wafer from tungsten-dominated particles produced on their surface. For wafer 3 and 4 mounted on similar positions within the torus comparable dust compositions were determined aside of the contribution of copper-dominated particles, indicating toroidally symmetric distribution of dust produced during the plasma operation. The high abundance of copper-dominated particles on wafer no. 4 can be explained by 5 flakes with ECDs between 9.5 and 82.2 µm contributing alone 9.7 % of the particle covered area. Their contrast-rich morphology mislead the detection algorithm to register multiple particles. Due to their large size and outer morphology local melting of close-by copper-based compounds such as the upper passive stabilization loop (PSL) was identified as the associated production process. Although wafer no. 5 was on a comparable position comparable to those of wafer no. 3 and 4, several differences in the dust particle composition can be observed. There, an increased number of carbon flakes covered a proportionally larger area. The high abundance of carbon flakes can be explained by mechanical abrasion of material from the close by graphite ECRH mirrors. Similar to wafer no. 4 for copper here the detection of a small number of large iron-dominated particles lead to a coverage fraction twice as high as the typical value. Post-mortem investigation of the plasma facing surfaces in this segment identified an intense arcing region in line of sight of the dust collector as the most probable source of these large particles of resolidified stainless steel alloy.

The arithmetic mean diameter (d_{ave}) and geometric mean diameter (GMD) [16] were determined from the equivalent circle diameter distribution of each particle class including data from wafer no. 1, 3, 4 and 5. From the tungsten droplet size distribution function the mean tungsten droplet mass of 1×10^{-7} mg was calculated allowing an estimation of the total mass accumulated on the horizontal areas in the torus under the assumption of toroidal symmetry and homogeneous surface coverage. While under the inner heat shield a tungsten droplet number density of 121 mm^{-2} was determined for the sampled area of 7.5 mm^2 size on wafer no. 1, 242

tungsten droplets per mm^2 were registered on 41.4 mm^2 area analysed on wafer no. 3, 4 and 5 yielding an averaged area number density of 223 mm^{-2}. Therefore, 61 mg of tungsten droplets were estimated to cover all horizontal areas in AUG of about 2.8×10^6 mm^2 size after the 2009 campaign. For the AUG campaign 2008, a similar estimation was performed leading to an amount of 510 mg of tungsten spheres [3]. The large deviation can be explained due to the melting and complete ablation of the tungsten coating of one of the outer divertor tiles in campaign 2008 leading to a considerably increased tungsten particle density in the torus. Furthermore, in the previous investigations all tungsten particles with a diameter smaller than 5 µm were included in the group of tungsten droplets, whereas present investigations showed that only about 40 % of all tungsten particles belong to this species.

5. Summary and outlook

A time- and resource-effective algorithm allowing correct tracking of all particles identified in more than 50 consecutive frames even at high background illumination and particle density was realized. Benchmarking of the algorithm efficiency was achieved experimentally by producing particle trajectories with known characteristics via parallel plate RF discharges. While in-vessel migration of dust particles can be tracked via fast camera video analysis, knowledge about the production mechanisms and in-vessel dust composition can be accessed by statistical post-mortem analysis of the morphological characteristics and elemental composition of individual dust particles. Therefore, 5×10^4 particles trapped on silicon dust wafer collectors during campaign 2009 were analyzed, showing that two third of the total number of dust particles in AUG is consisting of tungsten-dominated droplets and flakes, carbon-dominated grains and flakes or boron-dominated flakes and crystallites confirming results of earlier dust collection campaigns [1,3]. Up to 11 % of the particles were dominated by iron droplets indicating arc discharge ablation of stainless steel in-vessel components and copper flakes most probably originating from local melting of the passive stabilization loop (PSL). A total mass of

61 mg of tungsten-dominated droplets was estimated to have accumulated on the horizontal areas during the 2009 AUG campaign.

Parallel to the analysis of fast camera movies recorded during the two previous AUG campaigns in order to verify results obtained earlier by the analysis of standard diagnostic camera videos [17] statistical analysis of stereoscopic measurements as conducted at NSTX [14] will start in the next campaign providing three dimensional particle trajectories and thereby access to information about the in-vessel dust migration. In addition, the sampling efficiency of the presented Si wafer collection method will be determined by investigation of the composition of dust collected directly after vessel opening via application of adhesive carbon tapes and filtered vacuum sampling at the areas close to the silicon wafer collector positions.

Acknowledgements

This work, supported by the European Community under the contract of Association between EURATOM, CEA, and the French Research Federation for fusion studies, was carried out within the framework of the EFDA Task Force on Plasma Wall Interactions. The views and opinions expressed herein do not necessarily reflect those of the European Commission. Financial support was also received from the French National Research Agency through contract ANR-08-JCJC-0068-01.

References

[1] J.P. Sharpe, V. Rohde, The ASDEX-Upgrade Experiment Team, A. Sagara, H. Suzuki, A. Komori, O. Motojima and The LHD Experimental Group, J. Nucl. Mater. 313-316 (2003) 455-459.

[2] J.P. Sharpe, P.W. Humrickhouse, C.H. Skinner, the NSTX Team, T. Tanabe, K. Masaki, N. Miya, the JT-60U Team and A. Sagara, J. Nuc. Mat. 337-339 (2005) 1000-1004.

[3] V. Rohde, M. Balden, T. Lunt and the ASDEX Upgrade Team, Phys. Scr. T138 (2009) 014024.

[4] A.Yu. Pigarov, R.D. Smirnov, S.I. Krasheninnikov, T.D. Rognlien, M. Rosenberg, T.K. Soboleva, J. Nucl. Mater. 363-365 (2007) 216-221.

[5] J.D. Martin, M. Coppins and G.F. Counsell, J. Nucl. Mater. 337-339 (2005)114-118.

[6] Y. Tanaka, R. D. Smirnov, A.Yu. Pigarov and M. Rosenberg, Phys. Plasmas 15 (2008) 073704

[7] P.W. Humrickhouse and J.P. Sharpe, Fus. Eng. Des. 83 (2008) 1721-1724

[8] A. Denkevits, Hydrogen/dust explosion hazard in ITER: Effect of nitrogen dilution on explosion behavior of hydrogen/tungsten dust/air mixtures, to be published in Fus. Eng. Des. (2010)

[9] C. Arnas, M. Mikikian, and F. Doveil, Phys. Rev. E 60, 7420 (1999).

[10] C. Zafiu, A. Melzer and A. Piel, Physical Review E, Vol. 63, 066403 (2001)

[11] Y. Zayachuk, F. Brochard, S. Bardin, J.L. Briançon, R. Hugon, and J. Bougdira, in preparation for Rev. Sci. Instrum.

[12] S. Bardin, J.L. Briançon, F. Brochard, V. Martin, Y. Zayachuk, R. Hugon and J. Bougdira, submitted to Contrib. Plasma Phys.

[13] J.H. Yu, D.L. Rudokov, A.Yu. Pigarov, R.D. Smirnov, N.H. Brooks, S.H. Muller, W.P. West, J. Nucl. Mat. 390-391 (2009) 216-219.

[14] W.U. Boeglin, A.L. Roquemore and R. Maqueda, Rev. Sci. Instrum. 79 (2008) 10F334.

[15] M. Sezgin and B. Sankur, J. Elec. Imaging 13 (2004) 146-165

[16] W.C. Hinds, Aerosol Technology: Properties, Behavior, and Measurement of Airborne Particles, 2nd ed., Wiley-Interscience, New York, 1999.

[17] S-H. Hong, C. Grisolia, V. Rohde and P. Monier-Garbet, Nucl. Fusion 50 (2010), 035002.

Figures & Figure captions

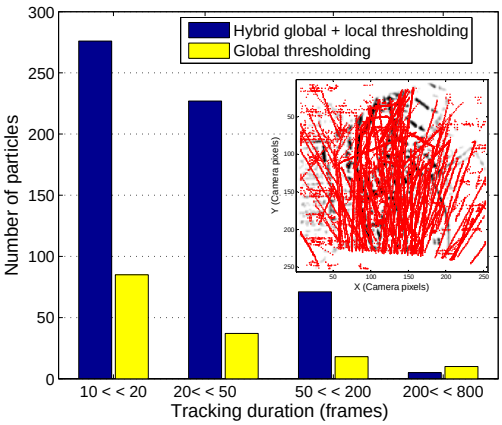

Fig. 1 In contrast to global thresholding hybrid global and local thresholding allows particle detection efficiencies of close to 100% and yields a 3-4 times higher number of identified particle fly-bys for tracking durations lower than 200 frames i.e. 20 ms. For longer tracking durations trajectories tend to be split. The insert shows in red the particles trajectories and hot spots observed during the first 1000 frames after a disruption superimposed to the AUG wall structures (ASDEX shot# 24002).

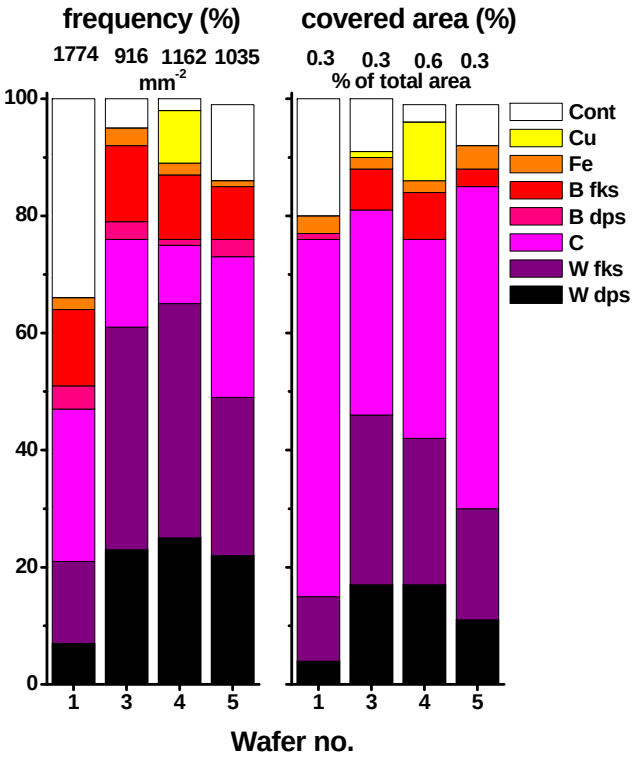

Fig. 2 left: The number of particles per class relative to the total number of particles on each wafer is given in % and the total number of particles per unit area is given for each wafer in mm^{-2} on top of each column; right: The fraction of the area covered by particles of one class relative to the total particle covered area is given in % and the total particle covered area relative to the total sampled area is given for each wafer in % on top of each column.

Tables & Table captions

Data mnts	W dps	W fks	C fks	B cls	B fks	Fe dps	Cu fks
d_{ave} (µm)	1.42	1.15	1.50	0.57	0.85	1.40	0.87
SE (µm)	0.01	0.01	0.03	0.01	0.02	0.11	0.04
GMD (µm)	0.29	0.41	0.20	0.02	0.08	0.01	0.02

Table 1 Arithmetic mean diameter (d_{ave}), its standard error (SE) and the geometric mean diameter (GMD) were determined for the seven particle classes identified on wafer no. 1, 3, 4 and 5. The abbreviations ‘dps’, ‘fks’ and ‘cls’ indicate droplets, flakes and crystallites.